Clays and Clay Minerals, Vol. 56, No. 2, 244–258, 2008.

THE OCCURRENCE AND GENESIS OF CLAY MINERALS ASSOCIATED WITH QUATERNARY CALICHES IN THE MERSIN AREA, SOUTHERN TURKEY

SELAHATTIN KADİR[1,*] AND MUHSİN EREN[2]

[1] Department of Geological Engineering, Eskişehir Osmangazi University, TR-26480 Eskişehir, Turkey
[2] Department of Geological Engineering, Mersin University, TR-33343 Mersin, Turkey

Abstract—Caliche in various forms, namely powdery, nodule, tube, fracture-infill, laminar crust, hard laminated crust (hardpan), and pisolitic crust, is widespread in the Mersin area in southern Turkey. It generally occurs within and/or over the reddish-brown mudstone of the Kuzgun Formation (Tortonian, Miocene) and alluvial red soils of the Quaternary. The mineralogical distribution along representative caliche profiles was examined by X-ray diffraction, scanning electron microscopy, differential thermal analysis-thermal gravimetry, and chemical techniques. Calcite is the most abundant mineral associated with minor amounts of palygorskite in caliche samples, whereas smectite is prevalent mainly in the reddish-brown mudstone and alluvial red soils of the caliche parent materials and is associated with appreciable amounts of palygorskite. These minerals are also accompanied by trace amount of illite, quartz, feldspar, and a poorly crystalline phase. Palygorskite fibers and fiber bundles were developed authigenically on euhedral or subhedral calcite crystals of the caliche units and at the edges of smectite flakes in the caliche host-rocks or sediments. Intense, continuous evaporation of subsurface soil-water resulted in an increase in pH and the dissolution of detrital smectite within the red mudstones and alluvial red soils that enclose the isolated caliche forms, and caused an increase in the Al+Fe and Mg/Ca ratio, favoring the formation of palygorskite under alkaline conditions. The calcium required for caliche formation may have originated from eolian dust, detrital carbonate minerals, and/or other caliche materials, which are dissolved by carbonic acid.

Key Words—Caliche, Geochemistry, Mineralogy, Palygorskite, Quaternary, Smectite, Turkey.

INTRODUCTION

Caliche (syn. calcrete) is defined as a near-surface terrestrial accumulation of predominantly calcium carbonate and palygorskite, as a minor component within sedimentary rocks, unconsolidated sediments, and soils. It occurs in a variety of forms, such as hardpan, laminar crust, powder, nodule, tube, and fracture-infill (Wright and Tucker, 1991). Arid and semi-arid climates are favorable for caliche formation because of the alternating wet and dry periods. In the study area, a Mediterranean-type semi-arid climate with a mean annual precipitation of 634 mm, a mean annual evaporation of 1321 mm, and an average annual temperature of 18.7ºC is dominant, and this led to widespread caliche formation in the region. Previous studies on caliche in Turkey are limited (Kapur *et al.*, 1987, 1990, 1993, 2000; Atalay, 1996; Atabey *et al.*, 1998). There is some information concerning the caliche-related palygorskite that was provided by Kapur *et al.* (1987) from the Adana region. Nevertheless, in the international literature, palygorskite authigenesis in caliches has received much attention (Singer and Norrish, 1974; Yaalon and Wieder, 1976; Galán and Ferrero, 1982; Inglès and Anadón, 1991; Rodas *et al.*, 1994; Verrecchia and Le Coustumer, 1996; Colson *et al.*, 1998; Khademi and Mermut, 1998; Pimentel, 2002). Therefore, this study was designed to describe palygorskite in the caliche units of the Mersin area in southern Turkey and to determine the relationships with abundant calcite and the host rocks and sediments rich in smectite. The origin of palygorskite is still the subject of debate.

MATERIALS AND METHODS

In all, 82 samples were collected from different types of caliche, such as powders, nodules, tubes, and fracture infills, and from their host sediments in the Mersin area. The mineralogical characteristics of the samples were further determined by X-ray powder diffractometry (XRD), differential thermal analysis-thermal gravimetry (DTA-TG), and scanning electron microscopy (SEM-EDX). The XRD analyses were performed using CuKα radiation at scanning speed of 1º2θ/min to determine the mineralogical compositions of the bulk samples.

Some samples were prepared for analysis by separation of the clay fraction (<2 μm) by sedimentation, followed by centrifugation of the suspension after dispersion overnight in distilled water. The clay particles were dispersed by ultrasonic vibration for ~15 min. Four oriented specimens of the <2 μm fraction from each sample were prepared by air drying, ethylene-glycol

* E-mail address of corresponding author:
skadir_esogu@yahoo.com
DOI: 10.1346/CCMN.2008.0560208

solvation at 60ºC for 2 h, and thermal treatment at 350ºC and 550ºC for 2 h, respectively. Semi-quantitative estimates of the rock-forming minerals were obtained by using the external standard method of Brindley (1980), whereas the relative abundance of clay-mineral fractions was determined using their basal reflections and the mineral intensity factors of Moore and Reynolds (1989).

Representative clay- and calcite-dominated bulk samples were prepared for SEM-EDX analysis by adhering the freshly cleaved surface of each sample to an aluminum sample holder with double-sided tape and thinly coating with a film (350 Å) of gold using a Giko ion coater. The DTA-TG curves were recorded using 10 mg of powdered sample in a Pt sample holder at an average rate of 10ºC/min with an alumina reference. Chemical analyses of 56 whole-rock samples were made using inductively coupled plasma atomic emission spectroscopy for major and trace elements, and inductively coupled plasma mass spectroscopy for rare-earth elements (*REE*) at ACME Analytical Laboratories, Ltd. (Canada). In these analyses, detection limits ranged from 0.01 to 0.1 wt.% for major elements and 0.1 to 5 ppm for trace elements.

GEOLOGICAL SETTING

The study area, located in the western part of the Adana Basin, comprises Tertiary and Quaternary units (Figures 1 and 2). The Tertiary units are the Karaisalı Formation (Burdigalian-early Serravallian), consisting of reef limestones, the Güvenç Formation (Burdigalian-Serravallian), consisting mainly of marine, gray marls intercalated with argillaceous limestones, and the Kuzgun Formation (Tortonian, Miocene), including, from base to top, reef-driven slope deposits, reef-cover deposits (limestone), marine, greenish mudstones and yellow sandstones, and ancient meandering river deposits, mainly reddish-brown mudstones of overbank deposits. These formations are overlain by Quaternary, hard, laminated crust (caliche hardpan), deltaic sediments, alluvial red soils, and recent alluvium and terrace sediments.

In the Mersin province, caliches are widespread and occur in a variety of forms, such as powder, nodule, tube, fracture-infill, laminar (softpan) crust, hard laminated crust (hardpan), and pisolitic crust in and/or over the Kuzgun Formation and alluvial red soils (Figure 3). The vertical arrangement of different caliche forms represents several caliche soils, which are subdivided into groups as mature and immature profiles (Eren *et al.*, 2004). The mature profiles comprise the isolated caliche horizon, including powder, nodule, tube, fracture-infill, and hard laminated crust, and in some cases also pisolitic crust (Figure 3a, 3b). The immature profiles consist mainly of isolated caliche layers and, rarely, laminated crust, which is very restricted (Figure 3d).

Caliche-calcite powders dominate around desiccation and depression fractures in alluvial red soils (Figure 3e), and generally occur as white mottling 1 cm in diameter, or as coarse calcite powder of soft and friable character in red soil. Caliche nodules occur mainly in reddish-brown mudstone of the Kuzgun Formation and in alluvial red soils as white, irregular subrounded to sub-ellipsoidal, soft to firm nodules 4–15 cm in diameter (Figure 3a–d); the nuclei of some of the nodules are mudstone relicts. Caliche tubes are observed under the hardpan level as white, elongate to lenticular, soft to hard lime powder accumulations, generally associated with caliche nodules in the reddish-brown mudstones of the Kuzgun Formation, and also in alluvial red soils (Figure 3b, 3d); these tubes are 4–10 cm wide and 20–70 cm long, in a few cases up to 1.5 m long. Caliche fracture-infills occur in reddish-brown and green mudstones under the hardpan, resulting in a mesh-type texture and pseudo-fold-like structures, 2–6 cm wide and 20 cm–1.5 m long (Figure 3b).

The laminar crust is of white, laminar and locally, friable material, and is 25–90 cm thick in alluvial red soils, grading into a nodular and tubular horizon overlain by 40 cm-thick red soils (Figure 3e). The hard laminated crust (hardpan) is a gray to cream-colored, wavy carbonate crust ~1–1.5 m thick, with discontinuous laminae and exhibiting a tepee (pseudo-anticlinal) structure that covers different beds of the Kuzgun Formation (Figure 3a, 3b). Caliche fracture-infills are calcite infillings of non-tectonic fractures in red mudstones of the Kuzgun Formation below the hardpan. The pisolitic crust is ~70 cm thick (Figure 3f), overlying the hard laminated crust in a local area. The pisolites are poorly sorted, are brown on fresh surfaces, and have rounded to ellipsoidal structures. The pisolites are 2 mm–6 cm in diameter in the upper level, and 3 mm–2 cm in diameter in the lower level. The nuclei of some pisolites are empty because of dissolution.

RESULTS

XRD

The mineralogical composition of caliche, reddish-brown mudstone, alluvial soil-type host-rock, and sediment samples was examined by XRD. The results revealed that calcite is the predominant mineral, accompanied by a small amount of smectite, and, a locally minor palygorskite constituent in the caliche nodule, tube, fracture-infill, and powder samples, while predominant smectite is associated with slightly more palygorskite in the host-rock and sediment samples (Table 1, Figure 4). Accessory illite, quartz, and feldspar are also present in host-rock samples. Variations in the mineralogical composition of the samples are controlled by the degree of calichification and sampling. On the other hand, quartz, feldspar, and illite are either lacking or occur locally as accessories in caliche

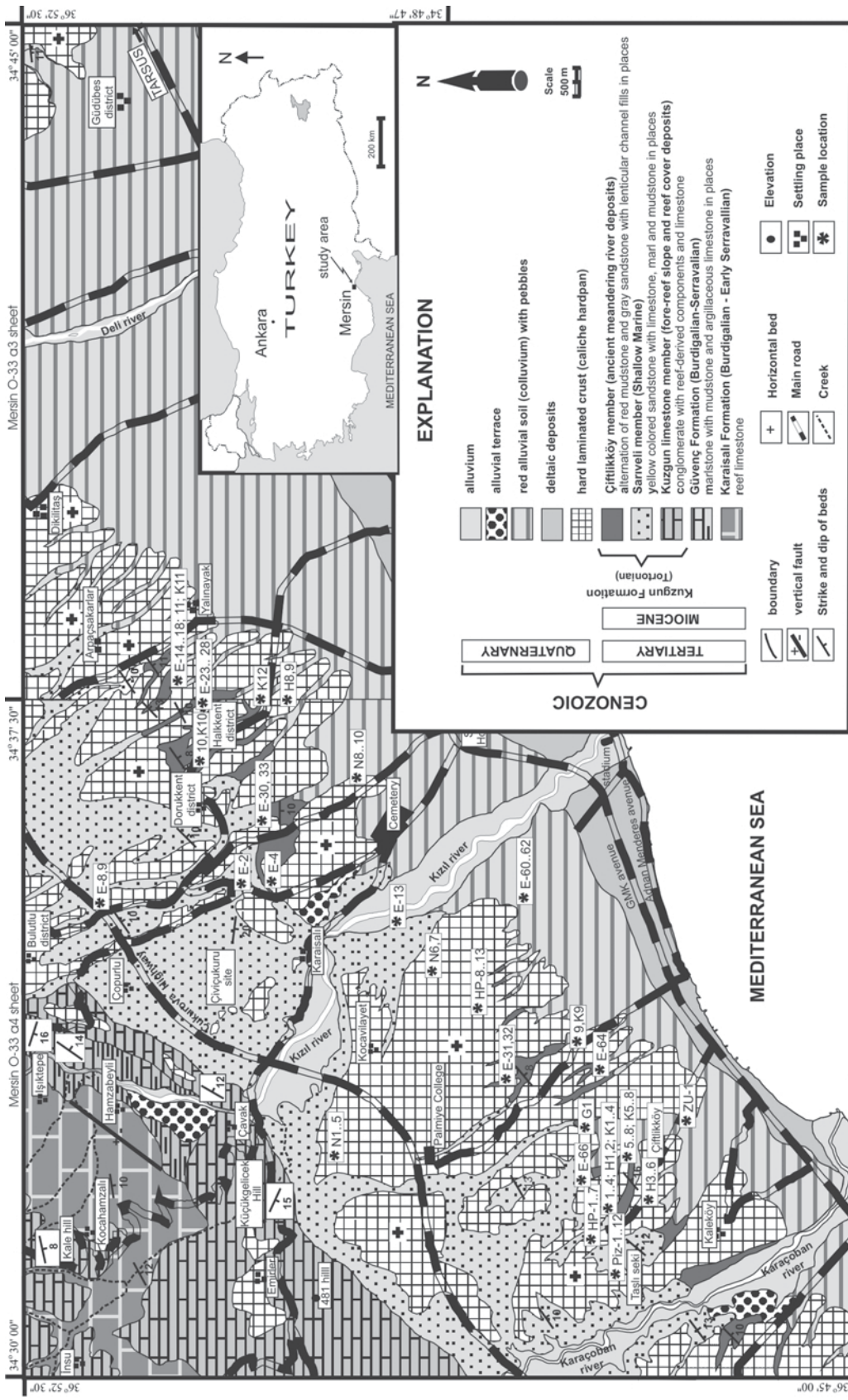

Figure 1. Geological map of the study area.

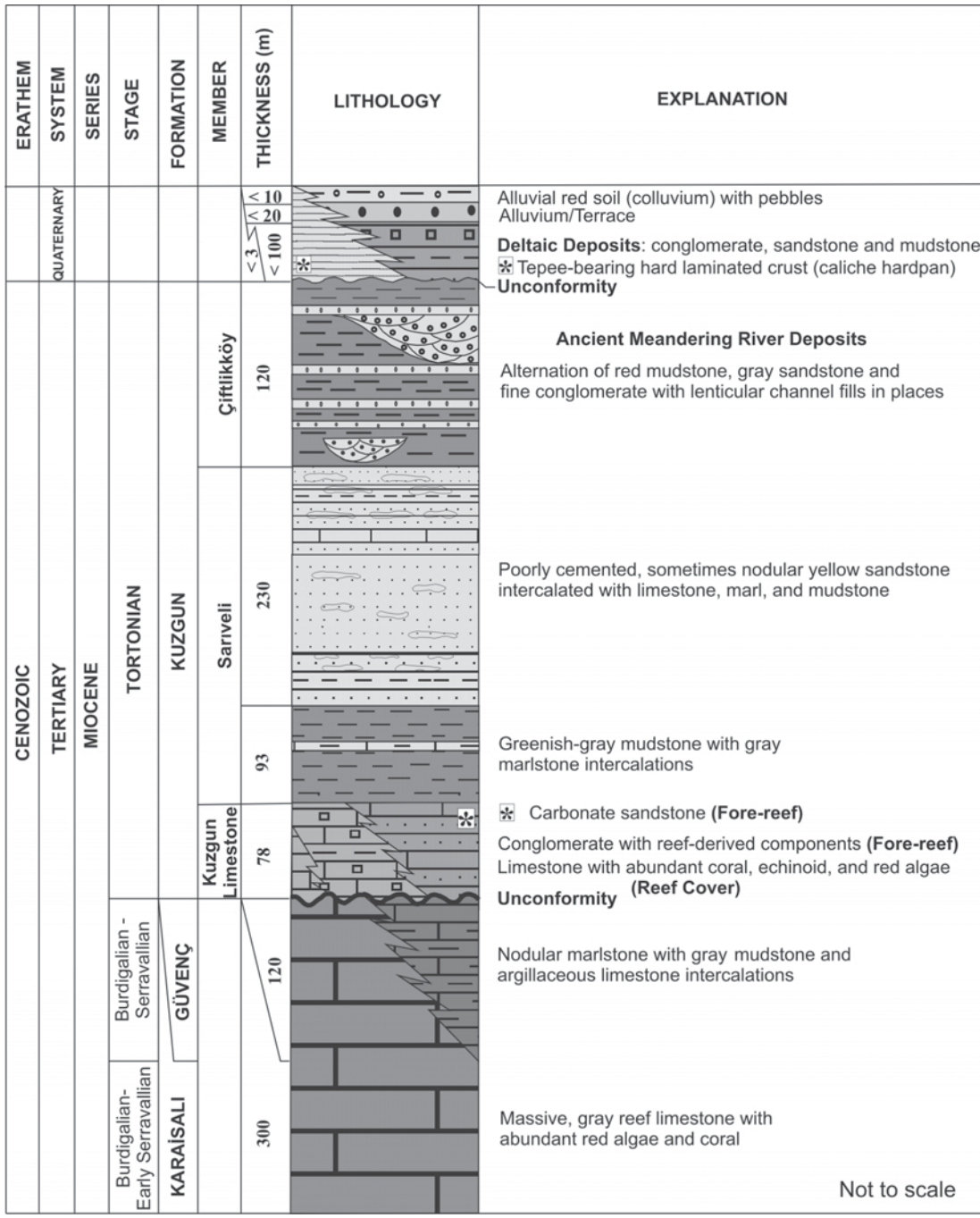

Figure 2. Generalized stratigraphic column section of the study area.

samples. In the hardpan samples, calcite predominates and dolomite is present as an accessory only in samples H-1 and H-5. Very small amounts of smectite were detected in these samples, whereas palygorskite and illite are either lacking or occur locally as accessories. Detrital quartz and feldspar are relatively abundant in comparison to the caliche powder, nodule, tube, and fracture-infill samples.

The 001 reflection peaks of palygorskite at 10.6 Å were not affected by ethylene-glycol treatment and collapsed upon heating to 350 and 550ºC for 2 h (Figure 4). However, the smectite 15.08–15.9 Å peaks expanded to 17 Å with ethylene-glycol treatment and collapsed to 10 Å with heating to 350ºC. Furthermore, additional heating to 550ºC caused a further reduction in sharpness and reflection intensity of the peak. The

smectite (*e.g.* smectite-rich K-11 samples) has a d_{060} value of 1.50 in the dioctahedral range.

The XRD background of most of the smectite- and palygorskite-bearing samples is slightly elevated, possi-

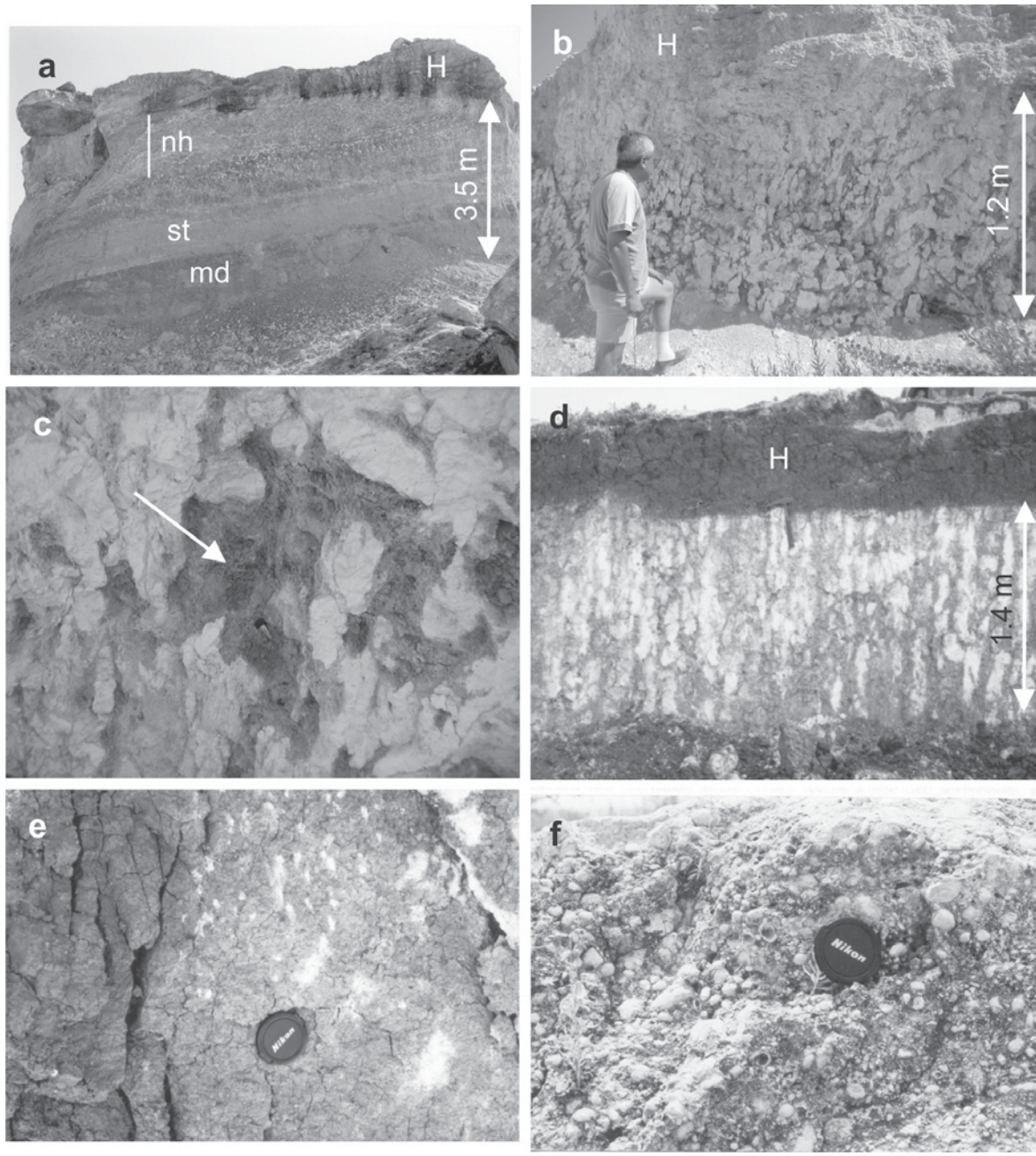

Figure 3. Field photographs showing caliche occurrences and profiles in the reddish-brown mudstone and alluvial red soils. (a) A typical maturated caliche profile showing hard laminated crust (H) overlying different beds of the Kuzgun Formation (large arrow), which grades into the nodular caliche horizon (nh: isolated caliche horizon; md: reddish-brown mudstone (overbank deposits; st: sandstone). Dorukkent quarter, Mersin. (b) A maturated caliche profile in which hard, laminated crust (H) grades into the nodular horizon (arrow showing isolated caliche horizon) within mudstone of the Kuzgun Formation, Çiftlikköy, Mersin. (c) A close-up view of the nodular horizon from part b in which white mottling indicates caliche nodules and the arrow shows a color change from reddish-brown to greenish-gray in the mudstone (scale bar (arrow) = 30 cm). (d) A typical immature caliche profile, including only the isolated caliche horizon (arrow), in alluvial red soil in which caliche nodules and tubes are common. Calcification resulted in a color change from reddish-brown to greenish-gray. The caliche horizon is overlain by recent soil cover (dark reddish-brown color). Foundation excavating wall in Akkent quarter, Mersin. (e) Caliche powders (white-mottling) in alluvial red soils, Akkent quarter, Mersin. (f) Pisolites in the pisolitic crust, Taşlıseki location, Mersin.

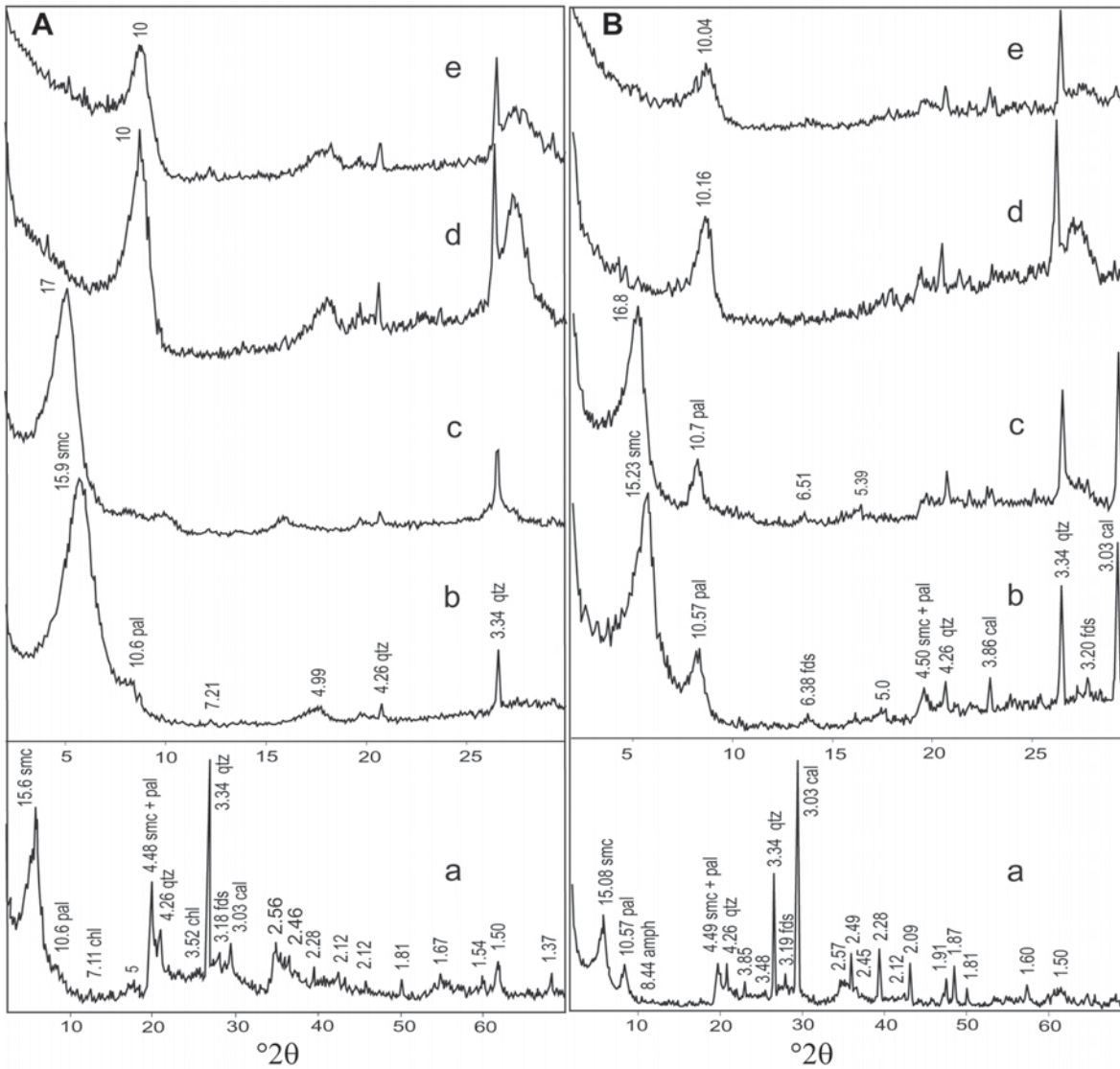

Figure 4. XRD patterns of the Mersin materials. (A) Smectite (K-11); (B) Palygorskite-bearing smectite (K-3) sample (a: powder; b: oriented; c: ethylene glycol-solvated; d: heated to 350ºC; e: heated to 550ºC). amph: amphibole; pal: palygorskite; smc: smectite; chl: chlorite; fds: feldspar; qtz: quartz; cal: calcite.

bly due to the presence of a poorly crystalline phase (Jones and Segnit, 1971; Iijima, 1980; Iijima and Tada, 1981). There is a positive relationship between the amount of the background increase, and the smectite and palygorskite content. Therefore, poorly crystalline and organic materials increased in the mudstone-hosted caliche powder in which smectite and palygorskite are dominant; conversely, these silicate clay minerals are absent or only accessories in the nodule, tube, fracture-infill, and hardpan samples in which calcite crystals are abundant.

SEM-EDX

Observations by SEM indicate that calcite rhombs are dominant in caliche samples and smectite is prevalent in reddish-brown mudstone and soil samples. Both exhibit distinct morphological shapes and associations with palygorskite. The caliche samples consist of euhedral or subhedral calcite crystals 4−10 μm in size, which are generally in close contact with each other (Figure 5a−d). The micropores among the calcite crystals comprise ~10% of the volume. Some palygorskite fibers and fiber bundles developed on calcite crystals (Figure 5a−d), and some of the calcite crystals have ellipsoidal forms ~5−10 μm in size. Individual palygorskite fibers are 0.5−3 μm long. Additionally, palygorskite fibers and fan-shaped fiber bundles developed at the edges of detrital smectite flakes of the host rocks or sediments, and also a small amount of smectite is present in caliche samples as a remnant of the host-rocks or sediments (Figures 5c−f).

The identification of calcite, palygorskite, and smectite crystals was based on XRD analysis, EDX

Table 1. Mineralogical variation in different types of caliche from the Mersin area.

Sample	Rock type	cal	dol	pal	smc	ill	qtz	fds
1-A	Caliche nodule	+++		+	+		acc	
1-B	Caliche nodule	++++			+			
2-A	Caliche nodule	++++		+			acc	
2-B	Caliche nodule	++++		+	acc		acc	
3	Caliche nodule	+++		+	+		acc	
4	Caliche nodule	+++		acc	++		acc	
5	Caliche nodule	+++			++	acc	accc	
6-A	Caliche nodule	++++			+			
6-B	Caliche nodule	++++		acc	+		acc	
7-A	Caliche nodule	++++			+			
7-B	Caliche nodule	++++			+			
8	Caliche nodule	+++			++		acc	
9*	Caliche tube	++++			+		acc	
10	Caliche nodule	+++		+	+		acc	
11-A	Caliche nodule	+++			+		acc	+
11-B	Caliche nodule	+++++						
12	Caliche nodule	+++++						
E-8	Caliche nodule	++			++	+	acc	acc
E-15	Caliche nodule	+++			++	acc	acc	acc
E-17*	Caliche tube	++			++	+	acc	acc
E-18*	Caliche tube	++++			+		acc	
E-20	Caliche nodule	+++			+	+	acc	
E-22**	Caliche fracture-infill	+++		+	+		acc	
E-23**	Caliche fracture-infill	+++		+	+		acc	
E-24**	Caliche fracture-infill	+++		+	+	acc	acc	
E-28	Caliche nodule	+++			+	+	acc	
E-29	Caliche nodule	+++			+	+	acc	
E-31	Caliche nodule	+++		+	+		acc	
E-32	Caliche nodule	++++		+				
E-60	Caliche nodule	++++			+	+	acc	
E-61*	Caliche tube	+++		acc	+	+	acc	
E-64	Caliche nodule	+++		+	acc	+	acc	
E-2*	Caliche tube	++++		acc	acc		+	acc
K-2*	Caliche tube	++++		acc	+			
C-1*	Caliche tube	++++		acc	acc			
G-1*	Caliche tube	+++		acc	+		acc	
K-9B*	Caliche tube	+			+++	+	acc	
ZU-1*	Caliche tube	+		acc	++++	acc	+	acc
E-62*	Caliche tube	+		+	++	acc	+	acc
Ps-4	Pisolite	+++++						
Ps-6	Pisolite	+++++					acc	
Ps-8	Pisolite	+++++						
Ps-9	Pisolite	+++++					acc	
Ps-10	Pisolite	+++++						
Ps-11	Pisolite	+++++						
Ps-12	Pisolite	+++++						
H-1	Hardpan	+++	+		+		acc	
H-2	Hardpan	+++			+		+	
H-3	Hardpan	+++		acc	+		+	
H-4	Hardpan	++++			+		acc	
H-4	Hardpan	++++					+	+
H-5	Hardpan	+++++	acc				acc	
H-6	Hardpan	++++			+		+	
H-8	Hardpan	+++++					acc	
H-9	Hardpan	++++		acc	+		acc	
HP-1	Hardpan	+++			+		+	+
HP-2	Hardpan	+++			+		+	
HP-3	Hardpan	+++			+		+	acc
HP-4	Hardpan	+++			+		+	+
HP-5	Hardpan	+++			+	acc	+	+
HP-6	Hardpan	+++		acc	+		+	+
HP-7	Hardpan	++++			acc		+	

Table 1 (*contd.*).

HP-8	Hardpan	++++	acc			+	
HP-9	Hardpan	+++	acc	+		+	
HP-11	Hardpan	+++		+		+	+
HP-12	Hardpan	+++		+		+	acc
HP-13	Hardpan	++++		acc		+	
K-1	Mudstone	+	++	++		+	acc
K-2	Mudstone	+	++	++		+	
K-3	Mudstone	+	++	++	acc	+	acc
K-4	Mudstone	+		++++	+	acc	acc
K-5	Mudstone	+	+	+++	acc	acc	acc
K-5B	Mudstone	acc	+	+++	+	acc	acc
K-5C	Mudstone	+	acc	++++	+	acc	acc
K-6	Mudstone	acc	acc	++++	acc	acc	acc
K-7	Mudstone	acc	+	+++	+	acc	acc
K-8	Mudstone			+++	+	acc	+
K-9	Mudstone	+	+	+++	acc	+	acc
K-10	Mudstone		++	+++	acc	acc	acc
K-11	Mudstone		acc	++++	acc	acc	acc
K-12	Mudstone	+	+	+++	acc	+	+
E-9	Mudstone	+	+	+++	acc	acc	acc
E-14	Mudstone	+	+	+++	acc	acc	acc
E-16	Mudstone	+	+	+++	acc	acc	acc
E-25	Mudstone	+	+	+++	acc	acc	acc
E-26	Mudstone	+	+	+++	acc	acc	acc
E-33	Mudstone	+	+	+++	acc	acc	acc
E-30	Mudstone	+	+	+++	acc	acc	acc

cal: calcite; dol: dolomite; pal: palygorskite; smc: smectite; ill: illite; qtz: quartz; fds: feldspar; +: relative abundance of mineral; acc: accessory.

spectral analysis of each individual crystal, and SEM examinations. The EDX analyses of rhombic crystals revealed a strong Ca peak used to identify calcite (Figure 6). Fibrous palygorskite and flaky smectite were determined by their strong Si, moderate Al, and smaller Mg and Fe peaks (Figure 6). The Al, Fe, and Mg peaks of smectite are slightly higher than those of palygorskite. The strong Ca peaks in these samples may be due to nearby or overlapping calcite crystals.

DTA-TG

The DTA-TG analysis of the smectite-dominated sample, K-11, shows a large endothermic peak at ~132ºC (weight loss: 14.5%), a moderate endothermic peak at ~554ºC (weight loss: 3.3%), and a final small endothermic peak at 853ºC (weight loss: 1.0%) (Figure 7a). Similar peaks were provided by Mackenzie (1957), Imai *et al.* (1969), Smykatz-Kloss (1974), Paterson and Swaffield (1987), and Jones and Galán (1988).

The DTA-TG curves for the K-10 sample indicate that dehydration occurred at three main peaks and one weaker peak between 100 and 1099ºC and was attributed to the association of palygorskite with smectite in the sample. Similar determinations from palygorskite have been reported by Imai *et al.* (1969), Jones and Galán (1988), and Patterson and Swaffield (1987) (Figure 7b). The first large endothermic peak at ~120ºC (weight loss: 13.8%) corresponds to the loss of adsorbed and zeolitic water. The second intermediate endothermic peak at ~544ºC (weight loss: 3.5%) is due to the expulsion of bound water. Also, a very weak endothermic peak developed at ~250ºC, possibly due to the fact that the bound water is strongly coordinated with magnesium atoms within the palygorskite channels, and remains stable until it is expelled at 544ºC. The last small endothermic peak at ~846ºC (weight loss: 0.7%) is due to structural dehydroxylation. The last endothermic peak is immediately followed by a broad exothermic peak coinciding with the structural collapse of both smectite and smectite-palygorskite, as well as the possible poor recrystallization of enstatite or some poorly crystalline phase, as reported by Kulbicki (1959) and Imai *et al.* (1969).

The DTA-TG curve for sample H-8 has a large endothermic peak at ~887ºC (weight loss: 45%) due to the decomposition of $CaCO_3$ in the calcite structure (Figure 7c). This result is in agreement with the findings of Mackenzie (1957), Webb and Kruger (1970), and Smykatz-Kloss (1974).

Chemical analyses

The chemical analyses of the representative samples of caliche, and of their host rocks and sediments, are given in Table 2. These units consist mainly of CaO, SiO_2, Al_2O_3, Fe_2O_3, MgO, and K_2O, and chemical variations are due to the proportions of clay and non-clay minerals in the samples (Tables 1 and 2). The large CaO content and significant loss on ignition are

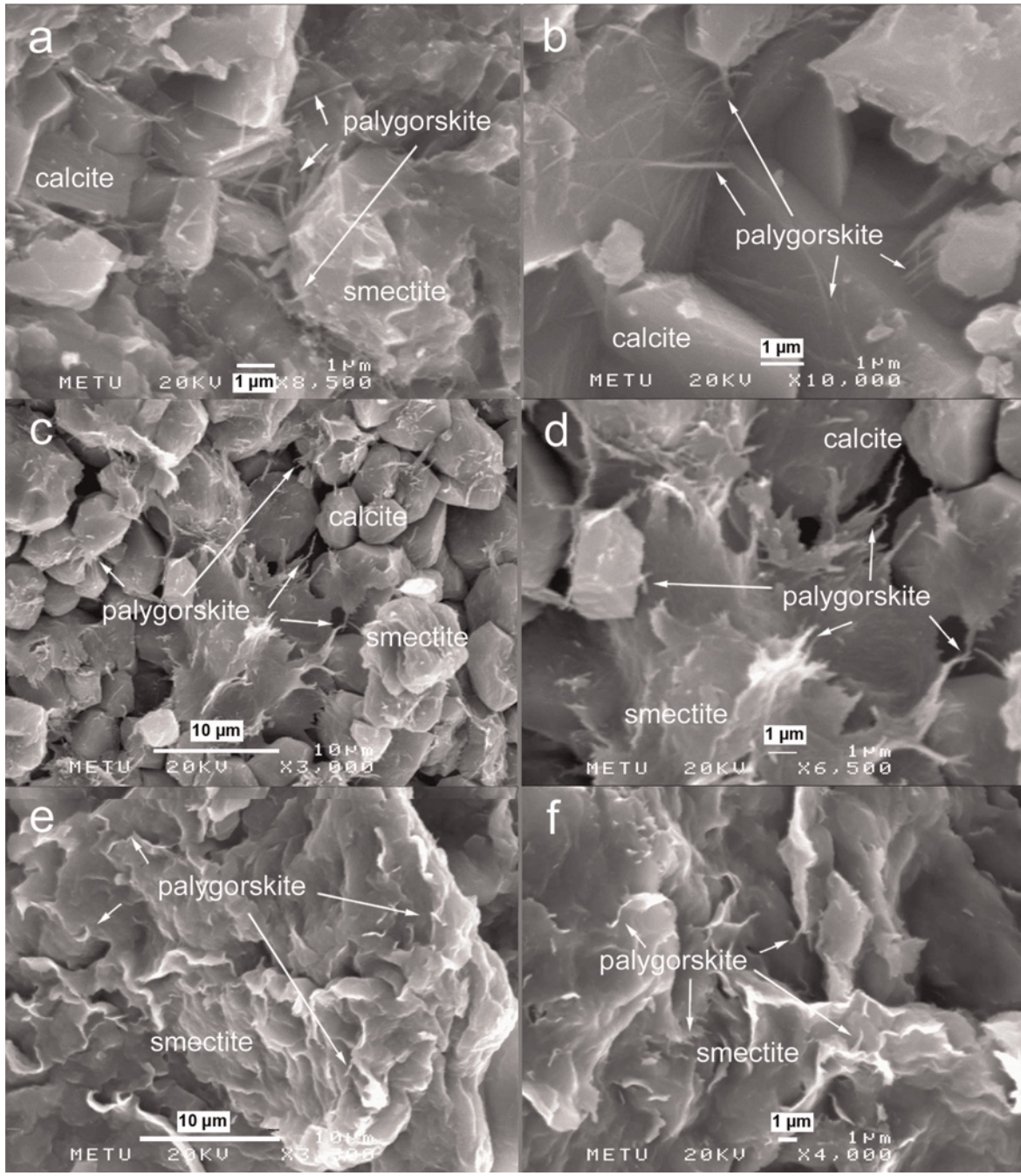

Figure 5. SEM images. (a) Development of palygorskite fibers between calcite crystals near smectite flakes (Piz-12). (b) Development of scarce individual palygorskite fibers on and between calcite crystals (Piz-12). (c) Elongate palygorskite fibers developed as cement between calcite crystals, and as fiber and fan-shaped bundles at the edge of smectite (3-2). (d) Close-up view of part c. (e) Close-up view of palygorskite fiber-edged smectite flakes (K-11). (f) Close-up view of the development of palygorskite fibers at the edge of smectite flakes (E-33).

attributed to the presence of calcite. The positive correlations between SiO_2, Al_2O_3, and Fe_2O_3, and relative increases in their abundances with increasing palygorskite and smectite in the samples reveal that both Al_2O_3 and Fe_2O_3 are bound within the structures of these minerals, as indicated by XRD, DTA-TG, and SEM. Furthermore, there is a relative increase in the red coloration of the mudstones with increasing Fe_2O_3 insofar as no other Fe phase or Fe-bearing minerals were detected (Eren and Kadir, 1999). The absence of

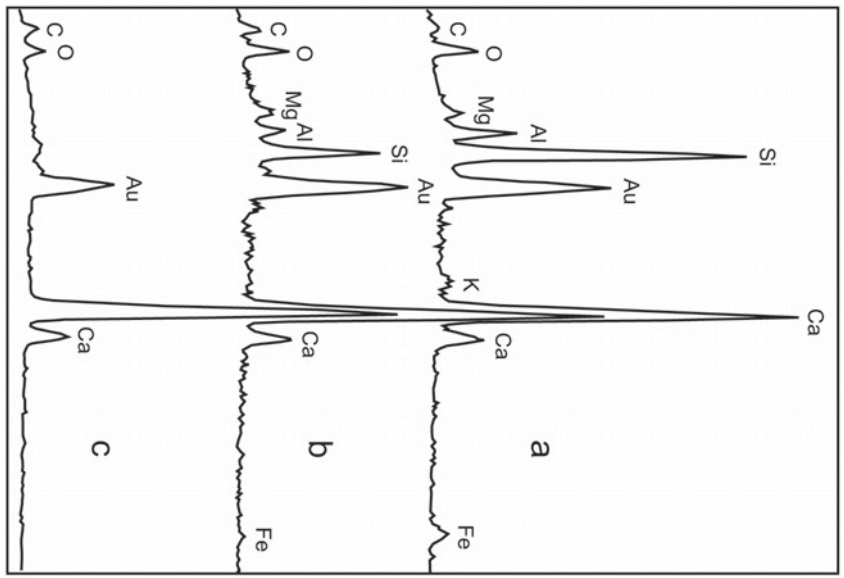

Figure 6. EDX analyses of caliche samples (a: smectite; b: palygorskite; c: calcite).

Mg-bearing, non-clay minerals in the samples indicates that Mg is associated with smectite and palygorskite. Therefore, the Mg content is inversely correlated with the degree of calcification. The K-11 smectite-rich mudstone sample is composed of 50.25% SiO_2, Al_2O_3+Fe_2O_3 (14.12% and 5.83%, respectively), 2.93% MgO, and 21.1% LOI. This chemical composition is similar to that of montmorillonite, as reported by Newman and Brown (1987).

The distribution of trace elements in the caliche units is in close agreement with their mineralogical compositions and major-element contents. The Zr, Cu, Zn, Ni, Co, Ce, Y, Nb, and Ta contents are notably small in the caliche samples with respect to red mudstone and red alluvial soil samples. The Zr and Zn exhibit only minor variations in the red mudstone samples, whereas the amount of Cu remains small and constant in the mudstone. The Co, Ni, and Cr are positively correlated with MgO and Fe_2O_3 in smectite- and palygorskite-dominated materials, and with trace ferromagnesian minerals in the red mudstone and alluvial soil samples, relative to the caliche samples.

The slight increase in TiO_2 in the red mudstone and alluvial soil samples is due to substitution of Ti for Fe. Niobium is constant, and immobile elements, Ce and Zr,

Table 2. Representative whole-rock, major- and trace-element abundances in caliche samples from the Mersin area (see Table 1 for rock types and mineralogical compositions of the samples).

	SiO_2	Al_2O_3	Fe_2O_3	MgO	CaO	Na_2O	K_2O	TiO_2	P_2O_5	MnO	Cr_2O_5	LOI	Total	Ba	Cu	Zn	Ni	Co	Sr	Zr	Ce	Y	Nb	Sc	Ta
K-1	42.25	9.00	5.21	3.14	14.28	0.11	1.66	0.45	0.03	0.08	0.034	23.7	100.03	141	39	37	172	24	164	54	41	10	<10	13	<20
K-2	41.15	6.60	3.04	2.40	20.18	0.30	0.90	0.35	0.02	0.07	0.047	24.8	99.94	141	22	<20	124	<20	282	64	26	<10	12	8	<20
K-3	39.64	9.47	5.68	3.51	14.42	0.15	0.86	0.52	0.06	0.08	0.026	25.4	99.91	83	46	34	195	25	185	61	40	10	<10	15	<20
K-4	43.82	11.68	6.30	3.09	10.10	0.19	1.06	0.60	0.05	0.09	0.023	22.9	100.01	166	44	53	192	26	184	77	65	10	<10	16	<20
K-5	42.46	11.19	6.61	3.41	10.61	0.14	1.60	0.57	0.05	0.08	0.030	23.1	99.95	148	37	53	238	26	170	64	30	10	<10	17	<20
K-5B	48.57	12.13	6.57	3.08	5.26	0.24	1.29	0.61	0.02	0.03	0.031	22.1	100.00	120	40	44	168	<20	79	73	<20	<10	<10	17	<20
K-5C	40.70	10.29	5.86	2.79	13.06	0.23	1.20	0.51	0.04	0.07	0.023	25.2	100.08	125	39	139	215	35	153	62	42	<10	<10	14	<20
K-6	47.67	12.02	6.48	3.20	6.01	0.24	1.16	0.60	0.02	0.08	0.032	22.4	100.01	131	32	53	219	24	83	86	64	<10	21	16	<20
K-7	48.27	12.09	6.07	3.46	5.02	0.20	1.69	0.58	<0.01	0.04	0.030	22.5	100.03	128	31	56	199	30	52	82	36	<10	<10	15	<20
K-8	53.35	13.71	2.65	4.22	2.66	0.29	0.56	0.30	<0.01	0.02	0.020	22.2	100.03	94	30	<20	46	<20	58	105	71	<10	<10	6	<20
K-9	43.93	11.34	5.50	1.46	12.76	0.17	1.43	0.61	0.01	0.07	0.054	22.6	100.03	194	30	50	145	22	88	129	61	13	12	13	<20
K-9B	46.71	12.26	6.07	1.45	10.25	0.26	1.60	0.69	0.01	0.08	0.062	20.5	100.04	188	25	53	195	22	67	144	81	14	10	15	<20
K-10	51.92	14.15	6.24	3.48	1.47	0.19	2.45	0.69	<0.01	0.03	0.045	19.3	100.03	171	39	55	86	<20	48	117	24	<10	<10	17	<20
K-11	50.25	14.12	5.83	2.93	3.46	0.12	1.49	0.58	0.01	0.02	0.033	21.1	100.01	109	45	58	76	<20	45	96	47	<10	10	16	<20
K-12	44.86	10.19	5.38	2.90	11.76	1.21	1.55	0.58	0.08	0.06	0.048	19.3	100.04	226	24	45	190	24	256	105	61	14	<10	13	<20
ZU-1	45.80	10.77	5.06	1.77	12.55	0.14	1.20	0.69	0.03	0.10	0.055	22.0	99.99	438	22	46	136	21	109	157	80	21	19	12	<20

Table 2. (*contd*.)

	SiO_2	Al_2O_3	Fe_2O_3	MgO	CaO	Na_2O	K_2O	TiO_2	P_2O_5	MnO	Cr_2O_5	LOI	Total	Ba	Cu	Zn	Ni	Co	Sr	Zr	Ce	Y	Nb	Sc	Ta
N-1	1.02	0.05	0.04	0.35	54.17	<0.01	<0.02	<0.01	0.02	<0.01	0.002	44.2	99.88	67	<20	<20	<20	<20	150	<10	<20	<10	<10	<1	<20
N-3	15.44	0.59	0.30	0.70	44.34	0.03	0.07	0.03	0.01	<0.01	0.003	38.4	99.97	107	<20	<20	<20	<20	202	<10	<20	<10	<10	1	<20
N-5	7.84	0.87	0.28	0.32	49.56	0.08	0.17	0.04	<0.01	0.01	0.010	40.7	99.91	63	<20	<20	<20	<20	125	15	<20	<10	<10	1	<20
N-8	2.82	0.70	0.39	0.36	52.30	0.03	0.06	0.03	<0.01	0.01	0.004	43.2	99.93	36	<20	<20	22	<20	75	<10	<20	<10	<10	1	<20
N-10	5.36	0.89	0.39	0.50	50.74	0.08	0.15	0.04	<0.01	0.01	0.009	41.8	100.02	62	<20	<20	38	<20	260	<10	<20	<10	<10	1	<20
H-1	1.72	0.49	0.26	0.29	53.35	<0.01	0.06	0.02	<0.01	<0.01	0.002	43.7	99.93	34	<20	<20	<20	<20	121	<10	<20	<10	<10	1	<20
H-3	3.62	0.59	0.26	0.33	52.17	0.03	0.13	0.03	<0.01	<0.01	0.006	42.8	99.99	47	<20	<20	<20	<20	121	<10	<20	<10	<10	1	<20
H-4	5.16	0.80	0.33	0.39	50.89	0.08	0.19	0.04	0.02	<0.01	0.008	42.1	100.04	65	<20	<20	<20	<20	141	20	<20	<10	<10	1	<20
H-5	3.50	0.58	0.24	0.28	52.18	0.04	0.13	0.03	0.01	<0.01	0.004	42.9	99.92	53	<20	<20	<20	<20	95	<10	<20	<10	<10	1	<20
H-8	1.03	0.24	0.12	0.32	54.22	0.02	0.04	<0.01	<0.01	<0.01	0.001	43.9	99.93	53	<20	<20	<20	<20	128	20	<20	<10	<10	<1	<20
H-9	3.01	0.77	0.39	0.39	52.10	0.02	0.11	0.04	<0.01	0.01	0.003	43.1	99.97	58	<20	<20	<20	<20	110	<10	<20	<10	<10	1	<20
E-4	7.06	0.77	0.19	0.34	50.09	0.07	0.22	0.03	<0.01	<0.01	0.007	41.2	100.02	72	<20	<20	<20	<20	194	10	<20	<10	<10	<1	<20
E-13	10.21	0.86	0.18	0.35	48.42	0.12	0.28	0.05	<0.01	0.01	0.027	39.5	100.05	125	<20	<20	<20	<20	174	37	<20	<10	<10	<1	<20
E-66	10.40	0.59	0.17	0.37	48.72	0.03	0.13	0.02	<0.01	0.01	0.006	39.6	100.07	78	<20	<20	<20	<20	163	<10	<20	<10	<10	<1	<20
A-1	7.81	1.44	0.69	0.55	48.92	0.02	0.25	0.07	0.01	0.01	0.008	40.2	100.00	26	<20	<20	20	<20	64	<10	<20	<10	<10	1	<20
K-3	2.85	0.45	0.25	0.45	52.51	0.01	0.05	0.02	<0.01	<0.01	0.003	43.4	100.03	20	<20	<20	<20	<20	135	<10	<20	<10	<10	<1	<20
G-1	2.86	0.59	0.32	0.42	52.69	<0.01	0.07	0.03	<0.01	<0.01	0.003	43.0	100.01	22	<20	<20	<20	<20	83	<10	<20	<10	<10	1	<20
K-1	2.83	0.65	0.31	0.53	52.08	0.02	0.06	0.03	0.01	<0.01	0.003	43.5	100.05	25	<20	<20	<20	<20	143	<10	<20	<10	<10	1	<20
8	5.19	1.26	0.26	0.64	50.84	0.04	0.07	0.03	<0.01	<0.01	0.004	41.7	100.05	15	<20	<20	<20	<20	77	13	<20	<10	<10	<1	<20
1-A	11.43	2.54	1.35	1.00	44.56	0.04	0.35	0.12	<0.01	0.02	0.012	38.5	99.97	39	<20	<20	49	<20	101	22	<20	<10	26	3	<20
B-3	7.01	1.04	0.34	0.43	50.21	0.07	0.23	0.04	<0.01	0.01	0.004	40.6	100.00	58	<20	<20	<20	<20	67	<10	<20	14	<10	1	<20
2-B	3.17	0.50	0.28	0.50	52.56	<0.01	0.04	0.03	<0.01	0.01	0.003	42.9	100.00	11	<20	<20	<20	<20	123	<10	<20	<10	<10	<1	<20
3	8.04	1.85	1.09	0.92	47.32	0.03	0.17	0.10	0.02	0.02	0.006	40.4	99.99	21	<20	<20	29	<20	132	<10	<20	14	13	3	<20
G-3	1.06	0.23	0.12	0.32	54.85	<0.01	0.02	<0.01	<0.01	<0.01	0.001	43.4	100.02	10	<20	<20	<20	<20	70	<10	<20	<10	<10	<1	<20
A-3	8.84	1.65	0.79	0.59	47.88	0.03	0.31	0.08	<0.01	0.02	0.008	39.9	100.11	35	<20	<20	26	<20	73	<10	<20	<10	<10	2	<20
B-1	3.06	0.75	0.43	0.38	52.41	0.04	0.08	0.04	<0.01	0.01	0.003	42.8	100.01	18	<20	<20	<20	<20	47	<10	<20	15	<10	1	<20
6-A	5.48	1.37	0.78	0.67	49.72	0.02	0.11	0.07	<0.01	0.01	0.003	41.7	99.97	19	<20	<20	26	<20	158	<10	<20	<10	10	1	<20
10	5.65	1.33	0.55	0.46	50.36	0.03	0.22	0.06	<0.01	0.02	0.004	41.4	100.10	19	<20	<20	<20	<20	54	<10	<20	11	<10	1	<20
9	9.07	2.43	1.23	0.52	46.89	0.04	0.30	0.14	<0.01	0.02	0.008	39.4	100.08	43	<20	<20	38	<20	50	22	<20	<10	12	3	<20
4	2.61	0.49	0.27	0.39	52.45	<0.01	0.04	0.02	<0.01	<0.01	0.002	43.6	99.90	14	<20	<20	<20	<20	85	<10	<20	<10	<10	<1	<20
2-A	5.73	0.84	0.46	0.70	50.68	0.03	0.08	0.04	<0.01	0.01	0.002	41.4	100.00	13	<20	<20	<20	<20	158	<10	<20	<10	<10	1	<20
11-B	1.10	0.31	0.12	0.25	54.71	0.02	0.03	0.01	<0.01	<0.01	0.003	43.4	99.97	14	<20	<20	<20	<20	50	<10	<20	<10	<10	<1	<20
7-A	3.57	0.96	0.51	0.47	52.10	<0.01	0.06	0.04	<0.01	<0.01	0.004	42.2	99.95	18	<20	<20	<20	<20	111	<10	<20	<10	<10	1	<20
5	6.10	1.12	0.56	0.56	50.08	0.03	0.08	0.05	<0.01	0.01	0.002	41.4	100.02	14	<20	<20	<20	<20	145	<10	<20	<10	<10	1	<20
Pz-7	2.90	0.52	0.36	0.82	51.14	0.01	0.07	0.03	0.01	0.04	0.009	44.0	100.03	44	<20	<20	30	<20	875	<10	<20	<10	<10	1	<20
Pz-8	0.55	0.08	0.42	0.93	53.46	0.04	<0.02	<0.01	0.01	0.04	0.002	44.2	99.90	44	<20	<20	<20	<20	1255	<10	<20	<10	<10	1	<20
Pz-9	0.92	0.14	0.32	0.74	53.32	0.01	0.03	<0.01	0.02	0.02	0.001	44.3	99.94	41	<20	<20	<20	<20	834	<10	<20	<10	<10	1	<20
Pz-10	0.79	0.15	0.48	0.84	53.28	<0.01	0.02	<0.01	0.02	0.02	0.003	44.2	99.93	50	<20	<20	23	<20	934	<10	<20	<10	<10	1	<20
Pz-11	0.93	0.18	0.39	0.82	53.37	<0.01	0.02	<0.01	0.01	0.01	0.002	44.1	99.96	47	<20	<20	<20	<20	851	<10	<20	<10	<10	1	<20
Pz12	0.72	0.14	0.42	0.82	53.54	0.03	0.02	<0.01	0.02	0.01	0.001	44.1	99.93	45	<20	<20	<20	<20	840	<10	<20	<10	<10	1	<20

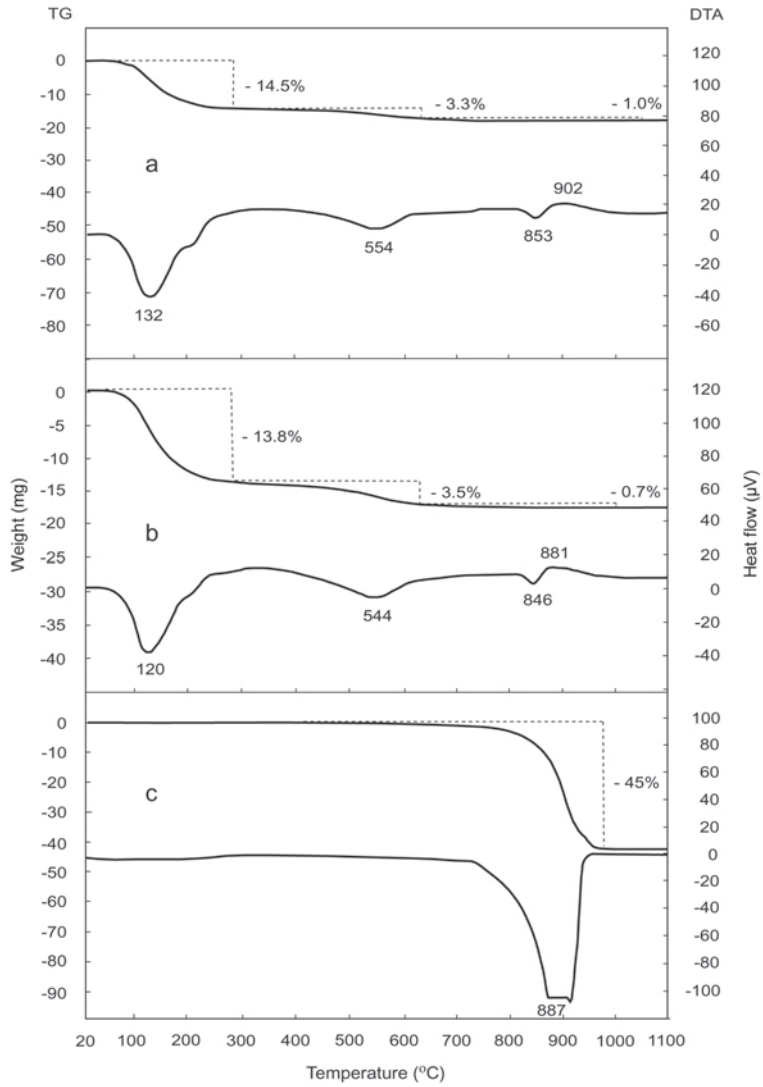

Figure 7. DTA-TG curves. (a) Sample of smectite-dominated green clay (K-11). (b) Sample of palygorskite-bearing smectite in gray clay (K-10). (c) Calcite (H-8).

correlate positively with K. Barium is generally greatest in the claystone samples (83−226 ppm), with the exception of sample ZU-1 (438 ppm), which shows a significant Ba content. In contrast, the caliches show small concentrations (11−65 ppm). The behavior of Ba is positively correlated with that of K; thus, it is related to the presence of illite and K-feldspar (the latter is associated mainly with clay minerals). The subparallel relationship between Ba and Sr indicates that both are present in similar minerals, insofar as Sr is concentrated in Ca-bearing minerals. Although the Sr content is variable, it increases significantly in the pisolite sample. This is due to the relative dominance of calcite (and possibly aragonite, which was below the detection limits in the samples) coupled with the possible evaporation and concentration of Sr-bearing water in small pits around tepee structures observed in pisolite accumulations.

DISCUSSION

Various caliche types, such as carbonate crust (hardpan), laminar crust, powder, nodule, tube, fracture-infill (softpan), and pisolitic crust, are widespread in the Mersin area. Local caliche-bearing profiles are dominated by calcite and accompanied by minor palygorskite. Smectite associated with palygorskite is increased, relatively, in the red mudstone and soil-type sediments of the caliche host rocks, which include traces of illite as well as accessory quartz and feldspars.

Calichification in the near-surface parts of the reddish-brown mudstone beds and its decrease downwards, and the presence of circum-granular and desiccation cracks, alveolar textures, caliche (vadose) pisolites, and vadose silts in the hard laminated crust all suggest formation in a vadose environment (Eren *et al.*, 2004). Eren *et al.* (2004) also reported calcite $\delta^{18}O$ isotope

values of samples ranging between −6.82 and −4.31‰ PDB, which indicates development under meteoric conditions. The calcite $\delta^{13}C$ values of the caliche samples ranging from −9.07 to −6.03‰ PDB and the biological features, such as alveolar textures, rhizoliths, caliche vadose pisolites, spherulite-like structures, calcite needles, and calcified filaments identified in the caliche hardpan by Eren *et al.* (2004), indicate a pedogenic origin of the caliches in the Mersin area.

The Mediterranean-type, semi-arid climatic conditions, with hot, dry summers and rainy, tepid winters, are favorable for caliche development in which evaporation exceeds precipitation (Goudie, 1983; Tucker, 1991). In this environment, during the wet period, CO_2-rich water, which is produced by decaying organic matter, roots, and microorganisms, filters downwards through permeable units and dissolves Ca-rich minerals. The released Ca- and CO_3^{2-}-bearing waters may infiltrate downwards, and are then subjected to intense evaporation. Calcite precipitates from meteoric soil water with a decrease in both CO_2 and H_2O as a result of high temperatures near the surface (Klappa, 1983). Downward movement of Ca-rich water along roots causes precipitation of $CaCO_3$ around the roots, resulting in the development of vertical pedotube-like structures and micrite coatings around grains. This, in turn, results in nodular structures and concentric coatings around grains, forming pisolites in places, as reported by Siesser (1973), Reever (1976), Hubert (1978), Semeniuk and Meagher (1981), Semeniuk and Searle (1985), and Beier (1987).

These environmental conditions are also favorable for the precipitation of palygorskite. After carbonate precipitation, palygorskite formed from infiltrating soil water through the intense, continuous evaporation of subsurface water under increased pH conditions, which leads to dissolution of detrital materials and aluminosilicates in red mudstones and soils. Microscopic determinations by SEM reveal that palygorskite fibers are elongate and have grown on and between carbonate minerals, showing the authigenically direct precipitation of palygorskite from solution under conditions of supersaturation, rather than a detrital derivation as reported by Hassouba and Shaw (1980), Allison and Riggs (1994), Gehring *et al.* (1995), and Akbulut and Kadir (2003). The association of palygorskite with smectite in the red mudstones and red alluvial soils, and the development of palygorskite at the edge of smectite flakes indicate that degradation of smectite was an important source for the precipitation of palygorskite, as outlined by Weaver and Beck (1977), Galán and Ferrero (1982), Singer (1979, 1984, 1989), Inglès and Anadón (1991), and Kadir (2007). Therefore, the relative abundance of palygorskite in caliche samples is related to the smectite content of the sample beacuse smectite provides Al and Si for palygorskite formation (Tables 1 and 2).

The data indicate a positive correlation between the chemical analysis and the expected mineralogical composition. Thus, red sediments contain larger amounts of Al_2O_3, Fe_2O_3, and MgO_2, as well as related Co, Ni, and Cr, and as smaller amounts of CaO and smaller LOI values than those of caliche samples, suggesting that smectite is the source of Al, Fe, and Mg for the precipitation of palygorskite (Tables 1 and 2). These results are also supported by the microchemical EDX analyses of smectite flakes, which revealed the presence of Si, Al, Mg, and Fe. Therefore, in the first stage following evaporation, calcite precipitation led to a decrease in Ca, and a relative increase in the Mg/Ca ratio and Al+Fe, favoring the precipitation of palygorskite from an alkaline solution. Furthermore, palygorskite formed in the same physicochemical environmental conditions by a dissolution-precipitation mechanism of precursor smectite.

The Ca required for calichification may have come from eolian dust, detrital carbonate materials, and from caliche itself, which were subsequently dissolved by carbonic acid, as reported by Goudie (1973), Reever (1976), and Eren *et al.* (2004). The increase in the poorly crystalline phase in the smectite- and palygorskite-rich caliche mudstone, as opposed to their absence or occurrence only as accessories in nodule, tube, fracture-infill, and hardpan samples in which calcite is abundant, may indicate that these materials were also the source of elements (Kadir and Karakaş, 2002), although some of the poorly crystalline phases contain organic matter. The carbon in CO_3 may come from organic matter. In fact pedologists have shown that the majority of C in carbonates comes from root respiration and decomposition of organic matter (Wright and Tucker, 1991; Oades, 1989).

CONCLUSIONS

Quaternary caliche units in the Mersin area are composed predominantly of calcite associated with small amounts of palygorskite. Detrital smectite associated with palygorskite, trace amounts of illite, quartz, feldspar, and poorly crystalline phase materials are often associated with these samples, and thought to be inherited from parent materials of the mainly reddish-brown mudstone (overbank deposits) of the Kuzgun Formation (Tortonian) and Quaternary red alluvial soils. Palygorskite developed on and between calcite crystals and at the edge of smectite flakes as fibers or fan-shaped fiber bundles, suggesting an authigenic origin. In caliches, calcite precipitation was driven by a decrease in CO_2 and H_2O as a result of evaporation, and was followed by palygorskite formation based on the extension of palygorskite fibers and fiber bundles from calcite crystals. The palygorskite formation reflects intense, continuous evaporation of subsurface soil water resulting in an increase in pH and the dissolution of detrital smectite in sedimentary rocks and soils. Intense evaporation produced high-pH (>8) conditions,

which resulted in the dissolution of pre-existing detrital smectite in the red mudstone and red alluvial soils, which in turn provided the high Mg/Ca ratio, and Al, Fe, and Si necessary for the formation of palygorskite from alkaline water by direct precipitation in association with calcite, or by transformation of precursor smectite to palygorskite.

ACKNOWLEDGMENTS

This study is part of a research project financially supported by the Scientific and Technological Research Council of Turkey (TÜBİTAK), under project number 102Y036 (Eren *et al.*, 2004). The authors are indebted to Professor Nuno L. Pimentel (University of Lisbon, Portugal) and an anonymous reviewer for their careful and constructive reviews, which improved the quality of the paper. We are also very grateful to Dr Warren Huff (University of Cincinnati, USA) and Dr Derek C. Bain (Macaulay Institute, UK) for their comments and suggestions.

REFERENCES

Akbulut, A. and Kadir, S. (2003) The geology and origin of sepiolite, palygorskite and saponite in Neogene lacustrine sediments of the Serinhisar-Acıpayam basin, Denizli, SW Turkey. *Clays and Clay Minerals*, **51**, 279–292.

Allison, M.A. and Riggs, S.R. (1994) Clay-mineral suites in cyclic Miocene sediments; a model for continental-margin deposition in a mixed siliciclastic-phosphatic-dolomitic-biogenic system. *Journal of Sedimentary Research*, **64**, 386–395.

Atabey, E., Atabey, N., and Kara H. (1998) Sedimentology of caliche (calcrete) occurrences of the Kırşehir region. *Bulletin of Mineral Research and Exploration*, **120**, 69–80.

Atalay, I. (1996) Palaeosols as indicators of the climatic changes during the Quaternary period in S. Anatolia. *Journal of Arid Environments,* **32**, 23–35.

Beier, J.A. (1987) Petrographic and geochemical analysis of caliche profiles in a Bahamian Pleistocene dune. *Sedimentology*, **34**, 991–998.

Brindley, G.W. (1980) Quantitative X-ray analysis of clays. Pp. 411–438 in: *Crystal Structures of Clay Minerals and their X-ray Identification* (G.W. Brindley and G. Brown, editors). Monograph **5**, Mineralogical Society**,** London.

Colson, J., Cojan, I., and Thiry, M. (1998) A hydrological model for palygorskite formation in the Danian continental facies of the Provence Basin (France). *Clay Minerals*, **33**, 333–347.

Eren, M. and Kadir, S. (1999) Colour origin of upper Cretacous pelagic red sediments within the Eastern Pontid, northeast Turkey. *International Journal of Earth Sciences*, **88**, 593–595.

Eren, M., Kadir, S., Hatipoğlu, Z., and Gül, M. (2004) Caliche development in Mersin area. TÜBİTAK Project, No.102Y036,136 pp. (in Turkish with English abstract).

Galán, E. and Ferrero, A. (1982) Palygorskite-sepiolite clays of Lebrija, southern Spain. *Clays and Clay Minerals*, **30**, 191–199.

Gehring, A.U., Keller, P., Frey, B., and Luster, J. (1995) The occurrence of spherical morphology as evidence for changing conditions during the genesis of a sepiolite deposit. *Clay Minerals*, **30**, 83–86.

Goudie, A.S. (1973) *Duricrusts in Tropical and Sub-tropical Landscapes*. Clarendon Press, Oxford.

Goudie, A.S. (1983) Calcrete. Pp. 93–131 in: *Chemical Sediments and Geomorphology* (A.S. Goudie and K. Pye, editors). Academic Press, London, New York.

Hassouba, H. and Shaw, H. F. (1980) The occurrence of palygorskite in Quaternary sediments of the coastal plain of North-West Egypt. *Clay Minerals*, **15**, 77–83.

Hubert , F.J. (1978) Paleosol caliche in the New Haven arkose, Newark Group, Connecticut. *Palaeogeography, Palaeoclimatology, Palaeoecology*, **24**, 151–168.

Iijima, A. (1980) Geology of natural zeolites and zeolitic rocks. Pp. 103–118 in: *Proceedings of the 5th International Conference on Zeolites* (L.V.C. Rees, editor). Heyden & Co., Naples, London.

Iijima, A. and Tada, R. (1981) Silica diagenesis of Neogene diatomaceous and volcaniclastic sediments in northern Japan. *Sedimentology*, **28**, 185–200.

Imai, N., Otsuka, R., and Kashide, H. (1969) Dehydration of palygorskite and sepiolite from the Kuzu District, Tochigi Prefecture, central Japan. Pp. 99–108 in: *Proceedings of the International Clay Conference*, Tokyo.

Inglès, M. and Anadón, P. (1991) Relationship of clay minerals to depositional environment in the non-marine Eocene Pontils Group, SE Ebro basin (Spain). *Journal of Sedimentary Petrology*, **61**, 926–939.

Jones, B.F. and Galán, E. (1988) Sepiolite and palygorskite. Pp. 631–374 in: *Hydrous Phyllosilicates (Exclusive of Micas)* (S.W. Bailey, editor). Reviews in Mineralogy **19**, Mineralogical Society of America, Washington, D.C.

Jones, J.B. and Segnit, E.R. (1971) The nature of opal I. Nomenclature and constituent phases. *Journal of the Geological Society of Australia,* **18**, 57–68.

Kadir, S. and Karakaş, Z. (2002) Mineralogy, chemistry and origin of halloysite, kaolinite and smectite from Miocene ignimbrites, Konya, Turkey. *Neues Jahrbuch für Mineralogie Abhandlungen*, **177**, 113–132.

Kadir, S. (2007) Mineralogy, geochemistry and genesis of smectite in Pliocene volcaniclastic rocks of the Doğanbey Formation, Beyşehir basin, Konya, Turkey. *Clays and Clay Minerals*, **55**, 402–422.

Kapur, S., Çavuşgil, V.S., Şenol, M., Gürel, N., and Fitzpatrick, E.A. (1990) Geomorphology and pedogenic evolution of Quaternary calcretes in the northern Adana Basin of southern Turkey. *Zeitschrift für Geomorphologie,* **34**, 49–59.

Kapur, S., Yaman, S., Gökçen, S.L., and Yetiş, C. (1993) Soil stratigraphy and Quaternary caliche in the Misis area of the Adana Basin, southern Turkey. *Catena,* **20**, 431–445.

Kapur, S., Saydam, C., Akça, E., Çavuşgil, V.S., Karaman, C., Atalay, I., and Özsoy, T. (2000) Carbonate pools in soil of the Mediterranean: A case study from Anatolia. Pp. 187–212 in: *Global Climate Change and Pedogenic Carbonates* (R. Lal, J.M. Kimble, H. Eswaran, and B.A. Stewart, editors). Lewis Publishers, Boca Raton, Florida.

Kapur, S., Çavuşgil, V.S., and Fitzpatrick, E.A. (1987) Soil-calcrete (caliche) relationship on a Quaternary surface on the Çukurova region, Adana (Turkey). Pp. 597–603 in: *Micromorphologie des Sols – Soil Micromorphology* (N. Federoff, L.M. Bresson, and M.A. Courty, editors). Association Française pour L' Etude du Sol, Paris.

Khademi, H. and Mermut, A.R. (1998) Source of palygorskite in gypsiferous Aridisols and associated sediments from central Iran. *Clay Minerals*, **33**, 561–578.

Klappa, C.F. (1983) A process-response model for the formation of pedogenic calcretes. Pp. 211–220 in: *Residual Deposits: Surface Related Weathering Processes and Materials* (R.C.L. Wilson, editor). Geological Society Special Publication **11**, Blackwell Scientific Publications, Oxford, UK.

Kulbicki, G. (1959) High temperature phases in sepiolite, attapulgite and saponite. *American Mineralogist*, **44**,

752–764.
Mackenzie, R.C. (1957) *The Differential Thermal Investigation of Clays*. Mineralogical Society, London, 456 pp.
Moore, D.M. and Reynolds, R.C. (1989) *X-ray Diffraction and the Identification and Analysis of Clay Minerals*. Oxford University Press, New York, 332 pp.
Newman, A.C.D. and Brown, G. (1987) The chemical constitution of clays. Pp. 1–128 in: *Chemistry of Clays and Clay Minerals* (A.C.D. Newman, editor). Monograph **6,** Mineralogical Society, London.
Oades, J.M. (1989) An introduction to organic matter in mineral soils. Pp. 89–159 in: *Minerals in Soil Environments* (J.B. Dixon and S.B. Weed, editors). Soil Science Society of America, Inc., Madison, Wisconsin, USA.
Paterson, E. and Swaffield, R. (1987) Thermal analysis. Pp. 99–132 in: *A Handbook of Determinative Methods in Clay Mineralogy* (M.J. Wilson, editor). Blackie and Sons Limited, Chapman & Hall, New York.
Reever, C.C.J. (1976) *Caliche*. Estacado Books, Lubbock, Texas, 266 pp.
Rodas, M., Luque, F.J., Mas, R. and Garzon, M.G. (1994) Calcretes, palycretes and silcretes in the paleogene detrital sediments of the Dueo and Tajo Basins, central Spain. *Clay Minerals*, **29**, 273–285.
Pimentel, N.L.V. (2002) Pedogenic and early diagenetic processes in Palaeogene alluvial fan and lacustrine deposits from the Sado Basin (S Portugal). *Sedimentary Geology*, **148**, 123–138.
Semeniuk, V. and Meagher, T.D. (1981) Calcrete in Quaternary coastal dunes in southwestern Australia: a capillary-rise phenomenon associated with plants. *Journal of Sedimentary Petrology*, **51**, 47–68.
Semeniuk, V. and Searle, D.J. (1985) Distribution of calcrete in Holocene coastal sands in relationship to climate, southwestern Australia. *Journal of Sedimentary Petrology*, **56**, 86–95.
Siesser, W.G. (1973) Diagenetically formed ooids and intraclasts in South African calcretes. *Sedimentology*, **20**, 539–551.
Singer, A. (1979) Palygorskite in sediments: detrital, diagenetic, or neoformed – a critical review. *Geologische Rundschau*, **68**, 996–1008.
Singer, A. (1984) Pedogenic palygorskite in the arid environment. Pp. 169–176 in: *Palygorskite-Sepiolite Occurrence, Genesis and Uses* (A. Singer and E. Galán, editors). Developments in Sedimentology **37**, Elsevier, Amsterdam.
Singer, A. (1989) Palygorskite and sepiolite group minerals. Pp. 829–872 in: *Minerals in Soil Environments* (J.B. Dixon and S.B. Weed, editors). Soil Science Society of America, Inc., Madison, Wisconsin, USA.
Singer, A. and Norrish, K. (1974) Pedogenic palygorskite occurrences in Australia. *American Mineralogist*, **59**, 508–517.
Smykatz-Kloss, W. (1974) *Differential Thermal Analysis, Application and Results in Mineralogy*. Springer-Verlag, Berlin, 185 pp.
Tucker, M.E. (1991) *Sedimentary Petrology: an Introduction to the Origin of Sedimentary Rocks*. Blackwell Science, Oxford, UK, 260 pp.
Verrecchia, E.P. and Le Coustumer, M.N. (1996) Occurrence and genesis of palygorskite and associated clay minerals in a Pleistocene calcrete complex, Sde Boqer, Negev desert, Israel. *Clay Minerals*, **31**, 183–202.
Weaver, C.E. and Beck, K.C. (1977) Miocene of the S.E. United States: a model for chemical sedimentation in a perimarine environment. *Sedimentary Geology*, **17**, 1–234.
Webb, T.L. and Krüger, J.E. (1970) Carbonate. Pp. 303–341 in: *Differential Thermal Analysis, volume 1, Fundamental Aspects.* (R.C. Mackenzie, editor). Academic Press, London and New York.
Wright, V.P. and Tucker, M.E. (1991) *Calcretes*. The International Association of Sedimentologists, Oxford, London, 352 pp.
Yaalon, D.H. and Wieder, M. (1976) Pedogenic palygorskite in some arid brown (calciorthid) soils of Israel. *Clay Minerals*, **11**, 73–80.

(*Received 30 July 2007; revised 20 December 2007; Ms. 0052; A.E. W. Huff*)